Supporting Information

Towards all-in fiber photodetector by directly bonding few-layer molybdenum disulfide to a fiber facet

Jin-hui Chen,[a] Zhao-huan Liang,[a] Lie-rong Yuan,[b] Cheng Li,[a] Min-rui Chen,[a] Yi-dong Xia,[a] Xue-jin Zhang,[a] Fei Xu*[a] and Yan-qing Lu[a]
[a]National Laboratory of Solid State Microstructures, College of Engineering and Applied Sciences and Collaborative Innovation Center of Advanced Microstructures, Nanjing University, Nanjing 210093, P. R. China
[b]School of Physics, Nanjing University, Nanjing 210093, P. R. China
*Corresponding authors email: feixu@nju.edu.cn

Supplementary Note 1: The fabrication process of all-in fiber photodetector (FPD)

Fabrication process of FPD is as follows. First, to remove the residual organic film in the fiber, a single-mode fiber protective coating was peeled off and was treated in ethanol with ultrasonic for a few minutes. Then, the fiber's end surface was cleaved and a flat platform on the facet was created. Second, the fiber was placed in film deposition equipment (K550X, EMTTECH) under vacuum (5×10^{-2} mbar) at a deposition speed of ~7.5 nm/min for 4 min. The facet gold film was scratched into a narrow channel using a sharp tungsten probe under an optical microscope, while the lateral electrodes were directly obtained by using a lapping film. The tungsten was fixed on a high precision moving stage. As a result, the moving process of a probe can be well controlled. In our scratching process, we first input a red light source into an optical fiber for guidance. Since the gold film's thickness is only ~30 nm, the red light can easily transmit over the thin film. The transmitted red light signal can be used for orienting the optical fiber core's position, with which we can quite precisely scratch the gold film into a small channel right on the fiber core position. Third, the MoS_2 on mica (Six Carbon Technology, Shenzhen, China) was transferred to a water surface by partially etching mica with 0.1 M NaOH. The MoS_2 was transferred to deionized water with a glass slide to ensure cleanliness. Finally, the MoS_2 was directly bonded to the fiber end surface using a dip-coating method. The as-fabricated FPD was annealed in a hot stage at 120℃ in air for 30 min to enhance the contact between the MoS_2 and electrodes.

Figure S1 is the optical microscope image of the lateral electrodes in fiber. The relatively smooth electrode gap was fabricated by moving two piece of lapping films (LF1P, Thorlabs) against a fiber coated with a thin layer of gold. Figure S2 demonstrates four typical image of fabricated electrodes on fiber facet. The electrode gaps cover from 4 μm-15 μm. Indeed, the electrode gaps depend on the size of tungsten probe. Figure S3

shows the typical optical image of as-fabricated FPD. We can find that after transferred a layer of MoS_2, the sample becomes pink, which can be attributed to the interference effect.[1] Similarly, graphene and WS_2 layers can also be transferred to the fiber facet as demonstrated in Fig. S3(c- d). Figure S4 is the SEM image of tyical MoS_2-based FPD.

The electric field distribution of fundamental mode (HE_{11}) in optical fiber at 400 nm wavelength is shown in Fig. S5a. It can be found that most of the light energy is confined in the core section. Figure S5b is the cut-line field distribution of Fig. S5a, which indicates the full width at half maximum (FWHM) of electric field intensity of HE_{11} mode is ~7.8 μm. As a result, the channel width of FPD should be designed at ~7-8 μm, considering the power collecting efficiency and the carrier's transition time in the channel.

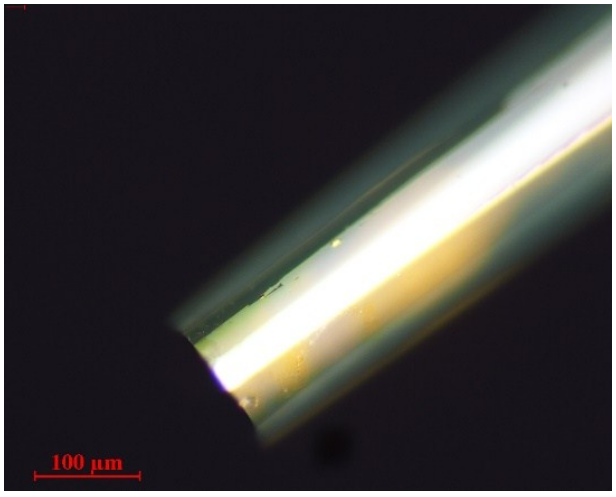

Fig. S1 The optical microscope image of lateral electrodes in fiber.

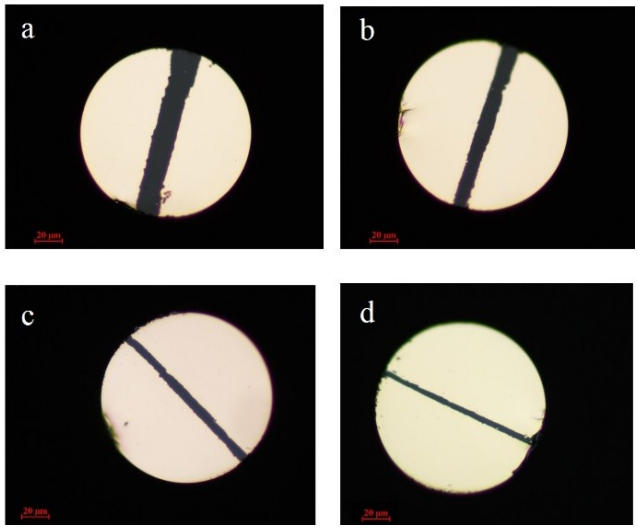

Fig. S2 The optical microscope image of electrodes on fiber end surface. The electrode gaps range from 4 μm-15 μm.

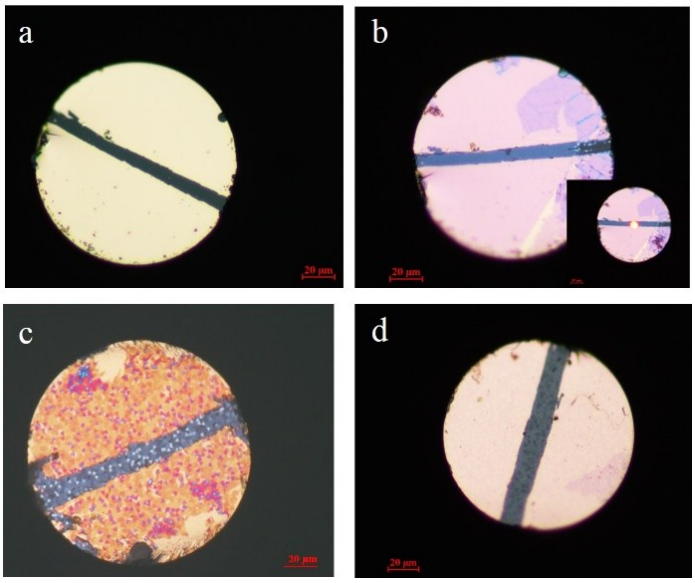

Fig. S3 Different 2D materials on fiber facet. (a) and (b) are samples with electrodes on fiber facet before and after transferred a layer of MoS_2. The inset in (b) is the sample launched with a red light source. (c) and (d) are samples transferred with few-layer WS_2 and multilayer graphene.

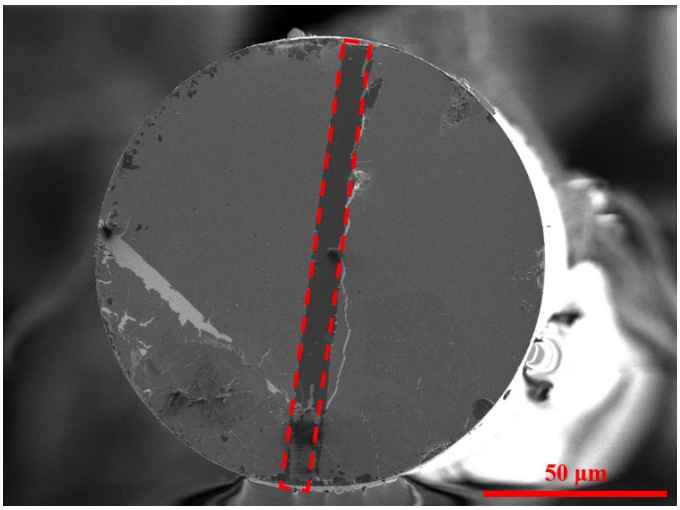

Fig. S4 The SEM image of the as fabricated MoS_2 film on a fiber facet with pair gold electrodes. The red dashed box shows the conducting channel of MoS_2.

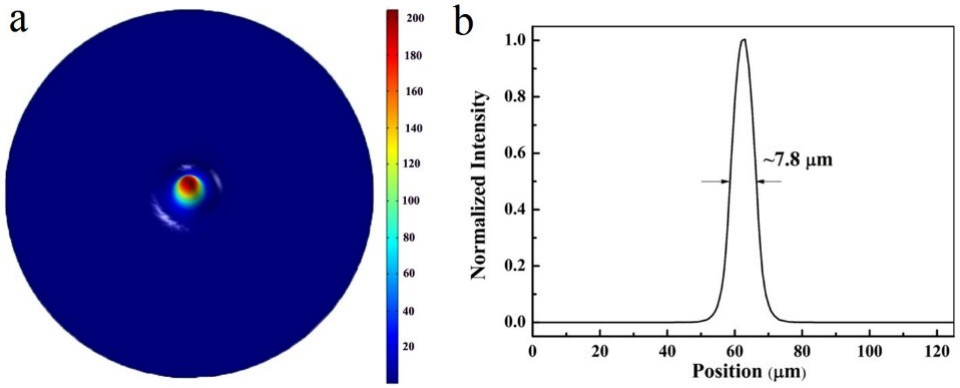

Fig. S5 Electric field distribution of HE11 mode in optical fiber. (a) The electric field distribution for HE_{11} mode in an optical fiber at 400 nm wavelength. (b) The center cut line of HE_{11} mode. The FWHM of HE_{11} mode is ~7.8 μm.

Supplementary Note 2: The optical characterizations of FPD

The few-layer MoS_2 was characterized by photoluminescence and Raman spectroscopy at room temperature in air (both measured on a LabRam HR 800 Evolution system, HORIBA Jobin Yvon) with an excitation line of 532 nm. We used gratings with 1800 gr/mm and 600 gr/mm for Raman measurement and PL characterization, respectively. The Raman band of the Si at 520 cm^{-1} was used as a reference to calibrate the spectrometer.

Here we in-situ measured the extinction spectrum (absorption & scattering) of FPD. The white light source (SLS201/M, Thorlabs) was directly launched into the FPD, and the transmitting light was collected by 20× object lens (NIKON) and analyzed by high sensitive spectrometer (NOVA, ideaoptics, China). From Fig. S6, we can find that our FPD has a considerably large absorption in 400-450 nm and a long absorption tail extends to 1000 nm.[2] The few-layer MoS_2 is an indirect bandgap semiconductor, thus the absorption spectrum usually shows long tails rather than the sharp edge as direct bandgap semiconductor. In addition, the absorption below the bandgap for MoS_2 is not a new phenomenon indeed. We find there are many papers reporting the near-infrared absorption of few-layer MoS_2.[3-5] The popular view on the absorption below the bandgap is that the stoichiometric ratio of Mo and S is not as precise as 1/2, thus crystal defects induce the redshift of the bandgap.[6] Since in our experiment, we used the CVD MoS_2, it is very likely that the non-stoichiometry reason that caused the long absorption tail. The small fluctuation imposed in the spectrum can be attributed to the mode interference effect and the electrodes edge scattering effects (Fig. S4).

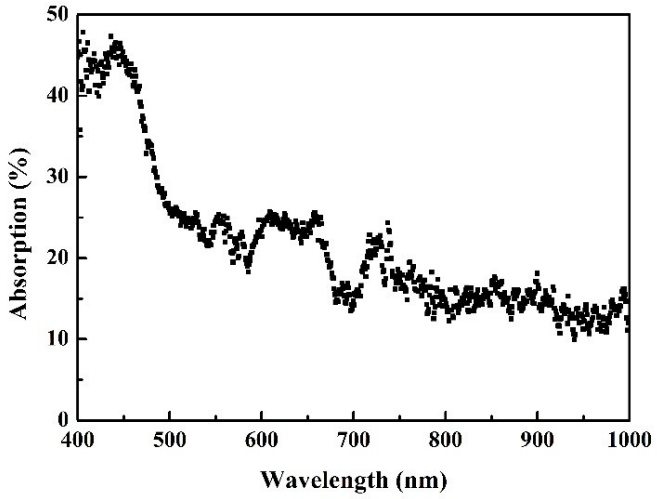

Fig. S6 The extinction spectrum of FPD in the visible and near-infrared band.

Supplementary Note 3: The photoelectrical characterizations of FPD

Different from an ordinary field-effect transistor (FET) on silicon, our photodetector was fabricated on a fiber end face. As a result, the illuminated light source was transported in the fiber waveguide and directly projected to the FPD at the output port without the need of lens systems. We used a homemade parallel metal plate to connect the fiber electrodes to exert bias voltage on the FPD. The photoelectrical characterizations were based on a sourcemeter (Keithley 2400) controlled by Labview programs. To calibrate to input power on the FPD, we used double arms configuration (referential arm and experimental arm), as illustrated in Fig. S7. The Keithley 2400 source meter is employed to exert bias voltage and analyze the current simultaneously, which is controlled by Labview programs.

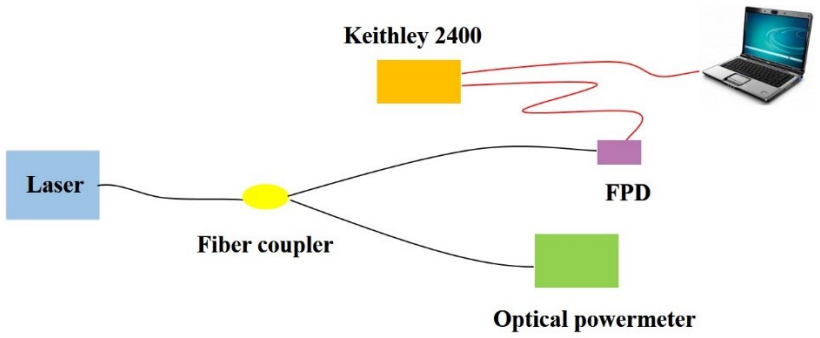

Fig. S7 The photoelectric characterization systems of FPD.

The contact resistances were measured by using the classical transfer length method (TLM),[7] as shown in Fig. S8. From linear fitting, we can find that the contact resistance

of the MoS_2-gold is ~48 GΩ·μm and the sheet resistance of MoS_2 is ~10 GΩ/□, which agrees well with previous reported CVD MoS_2-based device.[8] The relative high contact resistance can be attributed to the large sheet resistance and the Schottky barrier because of the work function mismatch. Theoretically, the Schottky barrier can be greatly reduced by optimizing the electrode structure and electrode materials,[9] such as Ti and Sc. And we believe that reducing the contact resistance can also enhance the device's performance.

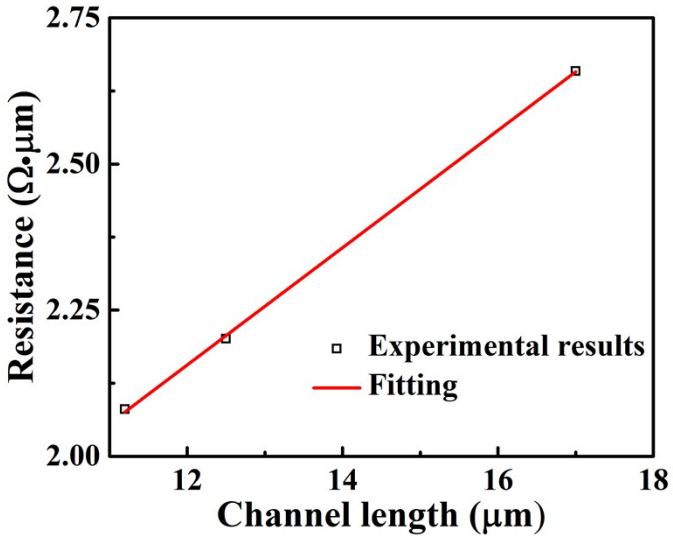

Fig. S8 Resistance versus MoS_2 channel length for gold-MoS_2 contact configurations.

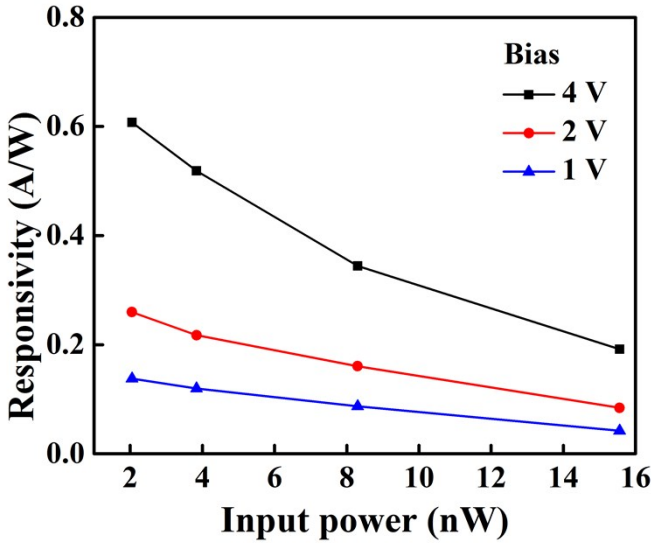

Fig. S9 The The photoresponsivity of the device versus the input power at different bias voltage with 532 nm light source.

Table 1 Figures-of –merit for MoS_2 based photodetectors

		Measurement conditions				Device performance		
Materials	Platform	V_{ds} (V)	V_g (V)	λ (nm)	P (mW/cm^{-2})	Responsivity (mA/W)	Rise time (ms)	Ref.
1 L MoS_2 (Exfoliated)	Si/SiO_2	1	50	532	8×10^{4}	7.5	5×10^{1}	10
1 L MoS_2 (Exfoliated)	Si/SiO_2	8	-70	561	2.4×10^{-2}	8.8×10^{5}	4×10^{3}	11
1 L MoS_2 (CVD)	Si/SiO_2	1.5	0	514.5	3.2×10^{4}	1.1	$\sim10^{3}$	8
1 L MoS_2 (CVD)	Si/SiO_2	1	41	532	1.3×10^{-1}	2.2×10^{6}	5×10^{5}	12
3 L MoS_2 (CVD)	**SiO_2 (optical fiber)**	**4**	**0**	**400**	**~7**	**6×10^{2}**	**7×10^{3}**	**This work**
5 L MoS_2 (PVD*)	Si/HfO_2	5	0	850	-	1.8×10^{3}	3×10^{2}	[4]

* DC magnetron sputtering

Supplementary Note 4: Discussions on the possible bias free working mechanism of FPD

Xue-tao Gan *et al*.[13], reported a technique that using spatial asymmetry electrodes to achieve photo-detecting without bias voltage with considerably high photoresponsivity ~ 0.015 A/W. Figure S10a shows the cross sectional structure of the chip-integrated graphene photodetector.[13] We can notice that one gold electrode is closer to the waveguide core position, while the other is further. As is known that when semiconductor contacts with metal, there exists strong built-in electric field because of the work function mismatch effect. Since one electrode couples more to the optical mode of waveguide, the built-in electric field will accelerate the photocarrier to the closer electrodes, thus creating net photocurrent. In our case, it is very similar to the phenomenon mentioned above. Figure S10b illustrates the schematic structure of our optical fiber integrated MoS_2 device (exaggerated viewing). We can see that very similar to Fig. S10a, one electrode is closer to the waveguide core, while the other is further. As a result, we figure that the closer electrode can couple more to the waveguide mode, while the other is not. Thus, the built-in electric field between the gold electrode and MoS_2 can ensure the acceleration of electrons (or holes) only in one direction and the absence of cancellation in the net photocurrent. Since in our device, there exist photogain effects because of the trap states,

the photoresponsivity can be also enhanced for bias free conditions. Further research is in need to completely clarify this issue.

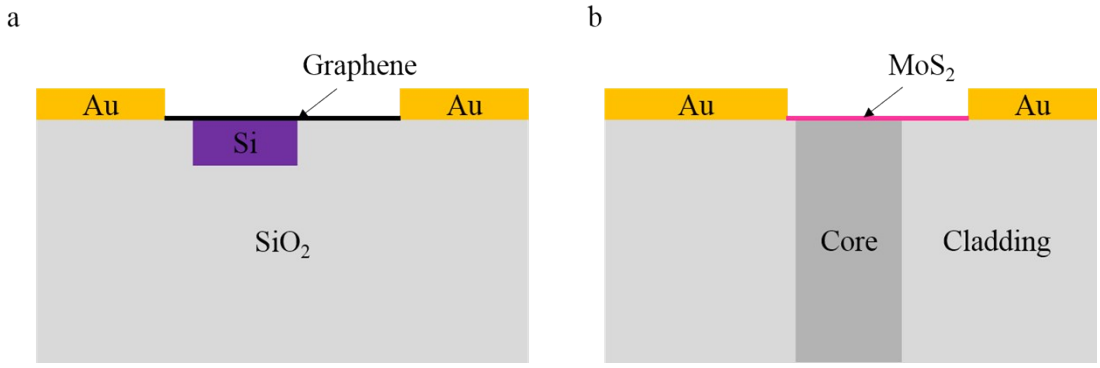

Fig. S10 The schematic strucutre of Ref.[13] and our device.

Supplementary References

1 H. Zhang, Y. Ma, Y. Wan, X. Rong, Z. Xie, W. Wang and L. Dai, *Sci. Rep.*, 2015, **5**, 8440.

2 W. Choi, M. Y. Cho, A. Konar, J. H. Lee, G. B. Cha, S. C. Hong, S. Kim, J. Kim, D. Jena and J. Joo, *Adv. Mater.*, 2012, **24**, 5832-5836.

3 W. Choi, M. Y. Cho, A. Konar, J. H. Lee, G.-B. Cha, S. C. Hong, S. Kim, J. Kim, D. Jena, J. Joo and S. Kim, *Adv. Mater.*, 2012, **24**, 5832-5836.

4 Z. P. Ling, R. Yang, J. W. Chai, S. J. Wang, W. S. Leong, Y. Tong, D. Lei, Q. Zhou, X. Gong, D. Z. Chi and K. W. Ang, *Opt. Express*, 2015, **23**, 13580-13586.

5 H. Zhang, S. B. Lu, J. Zheng, J. Du, S. C. Wen, D. Y. Tang and K. P. Loh, *Opt. Express*, 2014, **22**, 7249-7260.

6 S. Wang, H. Yu, H. Zhang, A. Wang, M. Zhao, Y. Chen, L. Mei and J. Wang, *Adv. Mater.*, 2014, **26**, 3538-3544.

7 R. Kappera, D. Voiry, S. E. Yalcin, B. Branch, G. Gupta, A. D. Mohite and M. Chhowalla, *Nat. Mater*, 2014, **13**, 1128-1134.

8 P.-L. Néstor, L. Zhong, R. P. Nihar, I.-R. Agustín, E. Ana Laura, M. Amber, L. Jun, M. A. Pulickel, T. Humberto, B. Luis and T. Mauricio, *2D Mater.*, 2014, **1**, 011004.

9 A. Allain, J. Kang, K. Banerjee and A. Kis, *Nat. Mater*, 2015, **14**, 1195-1205.

10 Z. Yin, H. Li, L. Jiang, Y. Shi, Y. Sun, G. Lu, Q. Zhang, X. Chen and H. Zhang, *ACS Nano*, 2012, **6**, 74-80.

11 O. Lopez-Sanchez, D. Lembke, M. Kayci, A. Radenovic and A. Kis, *Nat. Nanotechnol.*, 2013, **8**, 497-501.

12 W. Zhang, J.-K. Huang, C.-H. Chen, Y.-H. Chang, Y.-J. Cheng and L.-J. Li, *Adv. Mater.*, 2013, **25**, 3456-3461.

13 X. Gan, R.-J. Shiue, Y. Gao, I. Meric, T. F. Heinz, K. Shepard, J. Hone, S. Assefa and D. Englund, *Nat. Photon.*, 2013, **7**, 883-887.